JOURNAL OF MATERIALS SCIENCE 33 (1998) 1359–1367

The contributions of morphological and surface chemical modifications to the elevated-temperature ageing of copper–epoxy interfaces

B. J. LOVE
Department of Materials Science and Engineering, Virginia Polytechnic Institute and State University, Blacksburg, VA 24061-0237, USA

P. F. PACKMAN
Department of Mechanical Engineering, Southern Methodist University, Dallas, TX 75275, USA

Adhesion experiments were performed using both morphological and surface chemical modifications to identify whether one is dominant in controlling copper–epoxy adhesion and durability. Surface preparation procedures included sanding and etching copper surfaces which were thermally oxidized and a surface plating treatment that formed oxidized nodules on the copper surface. Further surface chemical modification used benzotriazole primary and chromium ion implantation on copper oxide. All prepared surfaces were laminated to an epoxy–glass resin cloth and the interfaces were aged in an air oven at 150 °C. Adhesion with ageing time was measured by a floating roller peeler assembly attached to a mechanical load frame. Interfaces formed when copper was oxidized in air had significantly lower peel strength than interfaces prepared by the plating treatment. Furthermore, peel adhesion was significantly reduced by elevated temperature conditioning. Adhesion degradation kinetics were applied to the transitional peel adhesion data and kinetic parameters associated with degradation at 150 °C were calculated. The results suggest that peel failure for the thermally oxidized samples occurs within the oxide layer, and that surface treatments on the oxide layer are not effective in altering adhesion. The peel adhesion of the electroplated surfaces was affected by the surface chemistry. No difference was observed in the fracture surface as a function of chemistry or ageing time.

1. Introduction

Copper–epoxy adhesion is key to the reliability of many types of electrical interconnects. Copper-based dielectric adhesion is of industrial interest, and there have been many research efforts whose goal has been to determine what factors lead to maximum adhesion. In most instances, this has led to many different aproaches using various adhesion promoters and resulted in questions about whether mechanical or chemical interactions control interfacial adhesion [1–9].

Studies of typical adhesion promotion schemes include wet chemical treatments such as oxidizing solution treatments (acidic and alkaline) and electroplating– anodizing schemes [1, 5, 7, 10–12]. Surface modifications have been attempted by exposure to organic bonding agents [4, 12–18] as well as dry chemical interactions such as ion implantation [19] and surface alloying [20].

Wet chemical treatments have used hot alkaline oxidizing treatments with oxidants such as sodium chlorite and hydrogen peroxide [1, 5, 7, 10–12, 21]. These treatments generate some level of surface roughness and increase the level of oxidation. Many of these efforts modified the concentration of the oxidizing species and time and temperature of exposure to identify the most effective bonding surface and there are a number of different treatments published in the research and patent literature. While many of these studies have resulted in increased adhesion, it is difficult to separate the morphological characteristics from the surface chemical characteristics as key contributors. This is essentially where research on other polymer–metal interfaces is centred. Buried in these research efforts are the questions of which particular oxide form and structure is most strongly bound to the base metal, which oxide form allows for physical and chemical interaction of the resin with the surface, and which particular oxide form and structure have either strong physical or chemical interactions with the curing epoxy resin system [10, 12, 21, 22].

There is a wide breadth of background information dealing with topographic modifications on metal

surfaces including aluminium, titanium and copper. Substantial amounts of information are available regarding oxide morphologies which occur on aluminium and titanium surfaces that allow for resin infiltration. With adequate resin infiltration and curing, the result is a relatively strong interface reinforced by a mechanically interlocking diffuse interphase region [6]. Evans and Packham [7] provided the most detailed mechanistic study of polymer–metal adhesion making use of copper, steel and zinc and found that similarly porous oxide forms that allowed for polymer infiltration within the formed oxide layer would dissipate larger amounts of peel energy, given that the yielding in the polymer layer would occur during debonding. Of course, their experiments also indicated reasonably strong base metal adhesion to the oxide layer.

More subtle surface modifications such as ion implantation and organic complexation agents tend to affect the surface chemistry but do not affect the bulk topography [4, 12–19]. Research on the adhesion of copper promoted by these more benign means has been done by polishing the copper surface to a mirror finish prior to surface modification. The mirror finish maximizes the surface chemical effect but the created surface may not reflect the behaviour of a realistic interface encountered in circuit board fabrication.

This research led to our own efforts to evaluate how surface modifications affected the peel strength and durability of realistic copper oxide surfaces formed from alkaline oxidizing solutions [23]. Surface modifications were performed on copper oxide surfaces with rougher topographies than the polished morphologies discussed by other researchers and changes in the adhesion of a chemically oxidized copper–epoxy laminated with time at elevated temperature [23]. The peel strength degradation with time at elevated temperature was tracked and degradation was found to relate well to the following expression:

$$\frac{A(t) - A(0)}{A(\infty) - A(0)} = \exp^{(-\Omega^* t)}$$

where $A(t)$ represents the peel strength after ageing for t h at a particular temperature (150 °C in this case), $A(0)$ and $A(\infty)$ represent the peel strengths immediately after lamination and after infinite exposure to the same elevated temperature as $A(t)$, respectively, and the degradation rate, Ω, relates to how fast degradation occurs and varied between 0.02 and 0.30 h^{-1} for the previous interfaces discussed.

This is derived by integration of the following kinetics expression for the adhesion degradation:

$$\frac{dA(t)}{dt} = [A(\infty) - A(0)]^*\Omega$$

We found that $A(\infty)$ tracked with the characteristic morphology and was independent of the surface chemistry in the limited number of surface treatments performed [23]. Further work has been performed with copper–epoxy interfacial durability by Yun *et al.* [2] and Hong and Wang [22] who have looked at the effects of elevated-temperature water immersions under different pH and ageing of the epoxy resin, respectively.

This paper reports an additional investigation of the contributions of morphology and chemistry by evaluating how the peel strength of other copper morphologies with characteristic oxide levels are affected when the substrates are modified using benign surface treatments prior to lamination with an epoxy resin. The oxide formation was initiated by two main processes: firstly air oxidation in an oven of etched and sanded copper surfaces and secondly a proprietary electroplating treatment which created a nodular morphology.

2. Experimental procedure

Electrodeposited oxygen-free high-conductivity (OHFC) copper foil (20.3 cm by 20.3 cm lateral directions by 0.071 mm thick) was obtained from Gould Inc. The copper foil was processed in three different ways. The different treatment processes are outlined below and are identified by sample numbers. The copper was received with a tarnish inhibitor on one side and a brass treatment on the other side. The copper side that was treated with the tarnish inhibitor was used to perform the metal treatment and the lamination to the epoxy resin.

2.1. Surface preparation and oxidation

Copper surfaces were prepared and oxidized as outlined in Table I.

In process 1, the foil was subjected to an extensive sanding with 180 grit sandpaper. There was significant sanding residue on the surface of the copper which was thoroughly rinsed with isopropyl alcohol. The samples were then dried with an air hose and placed in an air oven at 200 °C for time periods ranging from 15 to 60 min. The baked samples had a grooved microstructure and a characteristic morphology which is shown in a representative electron micrograph in Fig. 1. The scale of roughness is of the order of microns and it is observed to be without re-entrant cavities.

Process 2 removed the tarnish inhibitor through a pumice abrasion process. Following a deionized rinse and forced air drying, the copper foil samples were exposed to an aqueous $Na_2S_2O_g$ etchant solution using a conveyerized spray system. The etched samples were then rinsed and dried again using a forced-air dryer. The etched samples were then placed into an air oven at 200 °C and baked at various times ranging from 5 to 15 min. These baked samples had a pitted morphology and a representative electron micrograph is shown in Fig. 2. This microstructure has a characteristic roughness on the micron scale and is also devoid of reentrant cavities.

Process 3 used a proprietary plating treatment to alter the copper morphology similar to the work reported by Arrowsmith [1]. The foils were taped to a layer of laminate material in order to avoid exposing the plating bath to the brass side of the foil and were

TABLE I General outline of copper preparation conditions

Process condition	Surface preparation	Oxidation scheme	Surface chemical modification
1	180 grit sanding; isopropyl alcohol rinse; air dry	Air oxidation, 15–60 min at 200 °C	None
2	$Na_2S_2O_8$ etchant exposure; H_2O rinse; air dry	Air oxidation, 5–15 min at 200 °C	None
3	$Na_2S_2O_8$ etchant exposure; H_2O rinse; pumice abrasion	Three step plating process in a plating tank high in nitrates	None

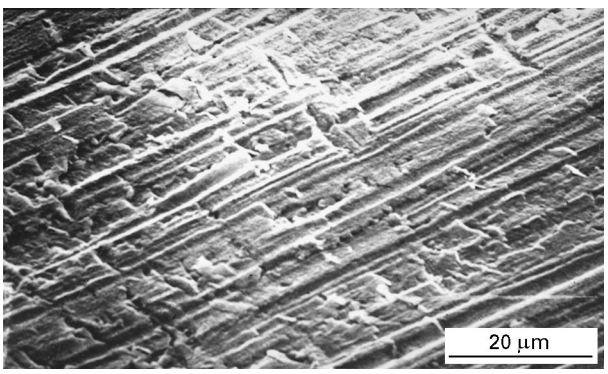

Figure 1 Electron micrograph of sanded copper morphology prior to oxidation.

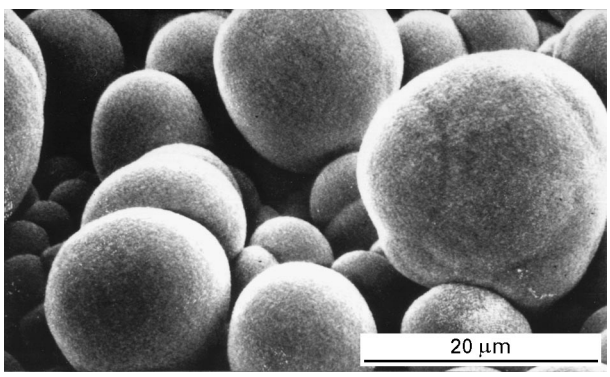

Figure 3 Electron micrograph of copper with the plated egg shell morphology prior to epoxy lamination.

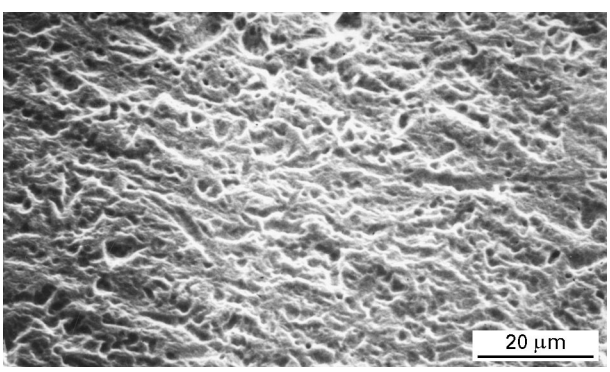

Figure 2 Electron micrograph of etched copper morphology prior to oxidation.

pumice abraded followed by exposure to the sodium persulphate. The foils were then rinsed in an alkaline cleaner, followed by 1 min in an aqueous bath of H_2O_2–H_2SO_4, immersion in a following rinse tank and then immersion in a plating tank. The plating tank was devoid of organic levelling agents and contained on average $CuSO_4$, (25 $g l^{-1}$) $NaNO_3$ (30 $g l^{-1}$) trace amounts of sodium ethylenediaminetetra–acetate (less than 1 $g L^{-1}$) and H_2SO_4 (75 $g l^{-1}$). By plating at very high current densities (greater than 500 $A m^{-2}$), an oxidized copper foil with a nodular morphology was formed. The morphological features of this plating are significantly larger than in the morphology generated by either process 1 or 2 and are shown in the electron micrograph in Fig. 3. Interestingly, there are re-entrant cavities which would be efficient microstructural anchors for infiltrating resin.

The foil oxidation mechanism is not completely understood. It is theorized that the lack of organic levelling agents and the high current densities in the plating bath limit the number of initiation sites over which deposition occurs. Those sites that initiate grow until they impinge upon one another. The presence of nitrates in the bath serve to oxidize the plating as the foil is exposed to the solution. Liquid chromatography analyses of the bath components found additional byproduct constituents confirming the reduction of nitrates in the bath.

2.2. Characterization

Scanning electron microscopy (SEM) and profilometry were conducted on all the surfaces to determine the surface characteristics of the foils. SEM was performed using a Cambridge 100 unit and a Tenupol diamond profiling unit was used for the profilometry measurements.

Surface analytical characterization was also performed on the samples to determine the level of oxidation. Auger electron spectroscopy (AES) made use of a Phi 595 scanning Auger microprobe equipped with an Ar^+ ion gun for depth-profiling studies. This instrument determined the level of oxidation on the surface both prior to lamination and following the peel testing to determine the locus of failure. Further surface analysis using X-ray photoelectron spectroscopy (XPS) was done with a Surface Science MK2 unit equipped with an attached hemispherical analyser and an Al Kα source. Survey scans were taken to determine the atomic concentrations of each element and high-resolution scans were taken to determine the valence structure of each element. Binding energies were set following the correction of the C 1s peak to 284.6 eV.

2.3 Surface modification

Following copper surface preparation and oxidation, some samples of the copper oxide were exposed to further chemical modification. The modifications included treatment by an organic priming process using an organic solution of benzotriazole or by Cr^+ ion implantation. The process schemes to form these specimen groups is shown in Table II.

The priming treatments were performed by making a 45 $g\,l^{-1}$ solution of benzotriazole in ethylene glycol. After the solution was uniformly mixed, each foil sample was immersed in the room-temperature solution. The solution was not mixed while the foil sample was immersed. The immersion period was 24 h. Following the immersion, each foil sample was rinsed substantially until it was clear that the ethylene glycol was rinsed off.

The Cr^+ ion implantation was performed at Implant Sciences (Danvers, MA USA). Each sample was exposed to a dose of 1×10^{16} ions cm^{-2} using an implantation energy of 40 eV. The maximum in the dose–depth profile of chromium into copper using the conditions outlined should be in the range of 17 nm. Penetration into copper oxide is thought to be rather different because of the differences in stopping power and density. Following the implantation procedure, no efforts were made to anneal implantation damage that may have been created during implantation. Further, since the implantation was done off line, the potential for surface contamination could not be ruled out following the completion of the implantation procedure before receiving them back.

2.4. Lamination

The copper oxide foil samples were then laminated to an epoxy–glass laminate using a partially cured epoxy-coated glass prepreg. The epoxy resin was a traditional FR4 brominated epoxy resin with a dicyandiamide curing agent. These samples were laminated at a temperature of 177 °C. Samples were heated under low pressure for about 5 min and then up to the 250 lbf in^{-2} for 1 h. Following the curing procedure, the samples were cooled under pressure where they were then removed from the lamination fixtures. Peel test samples were then cut and the rest of each sample was exposed to elevated temperature for various times to evaluate the effects of temperature ageing on adhesion.

Adhesion was evaluated using a floating roller peel tester. The unit was fixtured into an Instron 1123 screw-driven tensile tester and each sample was mounted and tested at a peel rate of 5.04 cm min^{-1}. Four samples were evaluated for each condition.

3. Results and discussion

3.1. Surface analysis results

The surface analysis results of the treated copper surfaces are shown in Table III for the XPS analyses and in Table IV for the AES analyses. Each oxidation procedure leads to oxide forms on copper that are different from our previous work on alkaline oxidizing solutions [23]. The level of oxidation created on specimens by process 1 changed as a function of the oxide depth. The high-resolution X-ray photoelectron emission spectrum around copper for the samples made by process 1 led to interpretation of Cu_2O formation and is

TABLE II Identification of specimen processing conditions

Process condition	Surface preparation	Oxidation	Surface modification
1A	Same as 1	Same as 1	Benzotriazole priming (45 $g\,l^{-1}$ in ethylene glycol) 24 h; H_2O rinse; air dry
1B	Same as 1	Same as 1	Ion implant,[a] 1×10^{16} Cr^+ cm^{-2}
3A	Same as 3	Same as 3	Benzotriazole priming (45 $g\,l^{-1}$ in ethylene glycol) 24 h; H_2O rinse; air dry
3B	Same as 3	Same as 3	Ion implant,[a] 1×10^{16} Cr^+ cm^{-2}

[a]Performed at Implant Sciences, Danvers, MA, USA.

TABLE III XPS analyses

Specimen	Amount of the following elements (%)				Other	Primary oxide by XPS
	Cu	O	C	Other		
1	28.2	27.5	37.9	6.5	N	Cu_2O
2	37.8	42.8	18.1	1.3	Cl, S	CuO
3	45.0	32.3	19.8	2.3	Cl, S	Cu_2O
1A	NT[a]					Assumed to be Cu_2O
1B	29.1	35.3	31.5	4.1	Cl, Sn	Cu_2O
3A	NT[a]					Assumed to be Cu_2O
3B	39.9	31.5	27.9	0.8	Cr	Cu_2O

[a]NT, not tested

TABLE IV AES analyses

Specimen	Amount of the following elements (%)				Other
	Cu	O	C	Other	
1					
2	48.0	27.4	21.1	4.7	Cl, S, N
3	69.4	26.0	1.7	2.9	Cl, S, N
1A	NT[a]				
1B	48.0	14.9	35.1	2	Cl
3A	NT[a]				
3B	40.6	9.1	42.9	6.3	Cl, N, S, Cr

[a] NT, not tested

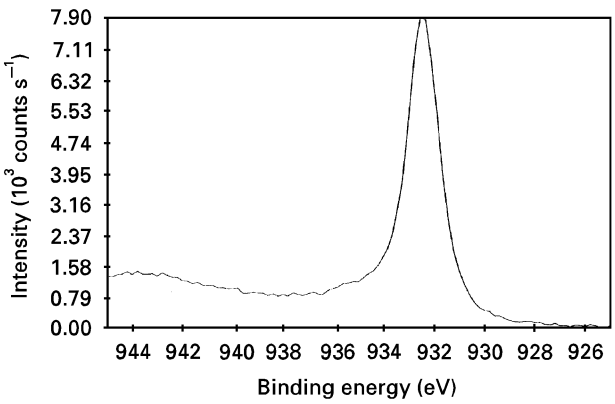

Figure 4 X-ray photoelectron emission spectrum expanded around copper for the sanded and oxidized specimen, prior to lamination.

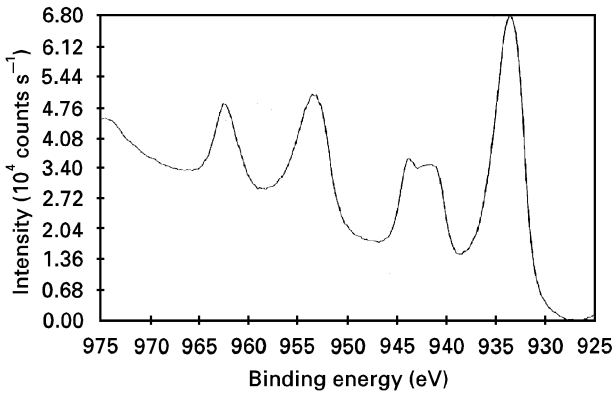

Figure 5 X-ray photoelectron emission spectrum expanded around copper for the etched and oxidized specimen prior to lamination.

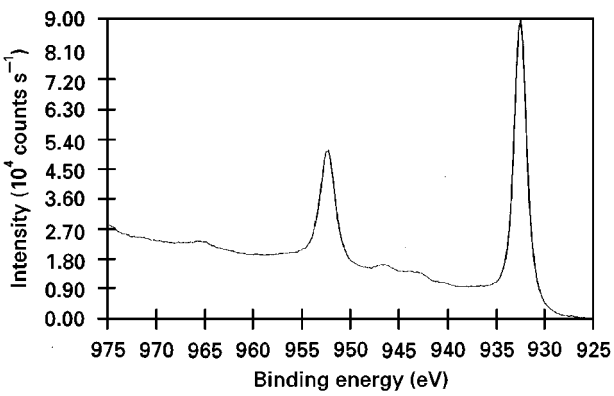

Figure 6 X-ray photoelectron emission spectrum expanded around copper for the egg shell plated copper specimen prior to lamination.

shown in Fig. 4. The primary Cu $2p_{3/2}$ is readily seen at 932.4 eV. The kinetic energy of the Cu $L_3M_{4,5}M_{4,5}$ Auger line occurs at 916.8 eV and corresponds to a copper binding energy of 569.8 eV. The primary XPS emission and the binding energy of the Cu Auger line at 569.8 eV are both confirmations of Cu_2O formation. The Cu-to-O ratio by AES increased with increasing oxidation time with a limiting ratio nearing 2-to-1 at long oxidation times, indicative of stoichiometric cuprous oxide. The Auger results also confirmed the atomic concentration findings and also showed a limiting ratio of 2 to 1 for the Cu-to-O ratio at long oxidation times. Simultaneous AES with Ar^+ depth profiling showed that these oxide films thicknesses ranged between 50 and 300 nm depending on the oxidation time. The average surface roughness was 0.4 μm.

Process scheme 2 resulted in the formation of CuO as determined by the XPS results in the copper region as shown in Fig. 5. The Cu XPS satellites for CuO at binding energies of 942 and 962 eV are clearly seen. These satellites were not observed on the sanded and oxidized samples. The primary Cu $2p_{3/2}$ emission is found at a binding energy of 933.2 eV and the kinetic energy of the Cu $L_3M_{4,5}M_{4,5}$ Auger line at 917.5 eV also confirms the oxide as CuO, although the hydroxide form could not be ruled out. The XPS results for an etched and air-oxidized sample even for 15 min at 200 °C in air found near the 1-to-1 ratio of elemental oxygen (counted as the sum of metal oxide forms) to elemental copper. The AES results showed less oxygen overall on the copper surface. It is clear that the surface preparation procedure affects the oxide formation process on the foil under air oxidation conditions. For samples processed according to process 2, the average surface roughness was 0.4 μm.

The surface analysis results for the electroplated surfaces (process 3) suggested that Cu_2O was forming on the outermost layer of copper, although the level of surface oxidation was much lower than for the thermally oxidized samples. The XPS emission for Cu $2p_{3/2}$ ws 932.4 eV. The kinetic energy of the Cu $L_3M_{4,5}M_{4,5}$ Auger line was found at 916.8 eV, confirming that Cu_2O is the prevalent species forming in the bath. A further confirmation for the lack of CuO is the absence of the satellite peaks at binding energies of 943 and 961 eV as is shown in Fig. 6. There were measurable amounts of chloride measured in the film as well as residual sulphur as a sulphate, which are residuals from the plating process in the copper sulphate plating tank. The AES results confirmed these additional constituents in the plating and the Ar^+ AES depth profiling determined the oxide thickness to be in the range of 10 nm. The average surface roughness was 4.0 μm, ten times larger than for the other two morphologies.

Surface analysis of samples that were ion implanted showed significant changes from the original surfaces. Samples that were implanted retained some level of native oxide on the copper surface which was indicative of cuprous oxide. A table of the XPS and AES surface analysis results for the samples baked for

10 min prior to ion implantation is shown in Table III. The table shows that the oxide has not changed on the surface but the amount of oxide has dramatically decreased. Estimates for the oxide thickness for the copper samples following implantation are less than 10 nm thick given the sputtering rate of 7.5 nm min^{-1}. Ion implantation has increased the surface Cu-to-O ratio from about 2.0 to about 3.1, further confirming a sputtering effect of the implanted Cr on the surface of the copper oxide. The etched oxide surfaces were not implanted given a better understanding of the overall mechanism of adhesion.

The surface analysis results for the implanted samples exposed to process 3 were more interesting. The level of oxidation is latent throughout the film. Even after sputtering for 40 min, there appears to be a chronic 7–10 at% O latent in the film, even after ion implantation. There also is a much higher concentration of non-copper oxide constituents in the film. On the implanted nodular surface, there is a relatively high concentration of carbon, probably as hydrocarbons. After implantation, copper remains in the form of Cu_2O.

3.2. Laminated peel strength results

The initial peel strength results (with no elevated-temperature ageing) for each process sequence are shown in Table V. There is a large difference between the initial peel strength of the air-oxidized copper interfaces and the strength of the plated surface. These results directly follow the work of Arrowsmith [1] who indicated that, the rougher the topography of the copper surface, the higher the resulting strength. There is also little difference in the peel strength between the preparation methods prior to air oxidation with only slight differences in laminated adhesion between the sanded surface and the etched surface. Surface modifications were also shown to have little effect in changing the adhesion to the epoxy resin. Only in the electroplated specimens which were then ion implanted was there any variation in the peel strength that was statistically significant.

More is learned by observing the fracture surfaces on the metal side of the failed interface. Representative photographs are shown for surfaces processed with the three different process morphologies in Figs. 7–9. Figs 7 and 8 show instances where residual polymer is clearly evident, but in few locations. The locations where residual epoxy is left over is dictated by the groove and etch patterns to which the epoxy flows at lamination temperatures. A very different failure is seen in Fig. 9 for the electroplated samples. Epoxy resin residue is clearly seen in the pits between nodules in the structure. Epoxy tearing is clearly more evident and is the mechanism responsible for higher overall peel strength.

The peel strength results for the laminated copper samples are shown as a function of ageing time of the interface in an air oven at 150 °C in Fig. 10. For the air-oxidized samples, there is a continued poor adhesion which is not a function of surface treatment. Each of these interfaces has poor adhesion over all exposure times. For the electroplated specimens, the initially large peel strength values are short lived as

TABLE V Initial peel strength results

Process type	Initial peel strength (N m^{-1})
1	0.18 (± 0.10)
2	0.29 (± 0.002)
3	2.02 (± 0.22)
1A	0.15 (± 0.05)
1B	0.52 (± 0.10)
3A	1.71 (± 0.35)
3B	1.01 (± 0.16)

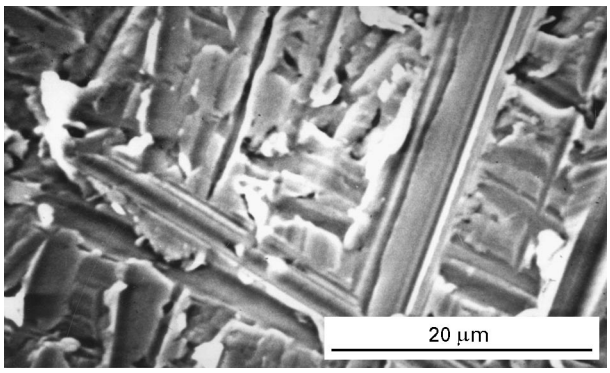

Figure 7 Electron micrograph of sanded and thermally oxidized copper surface following lamination to epoxy resin and peel testing.

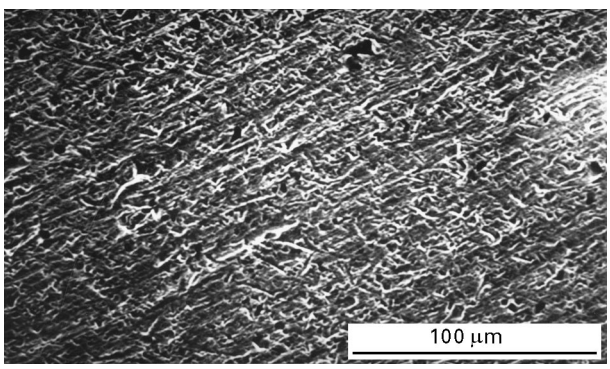

Figure 8 Electron micrograph of etched and thermally oxidized copper surface following lamination to epoxy resin and peel testing.

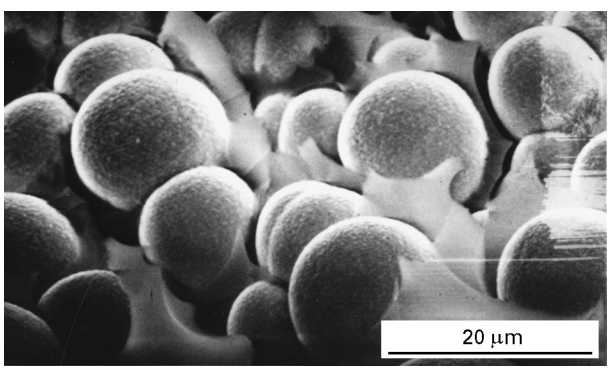

Figure 9 Electron micrograph of egg shell plated copper surface following lamination to epoxy resin and peel testing.

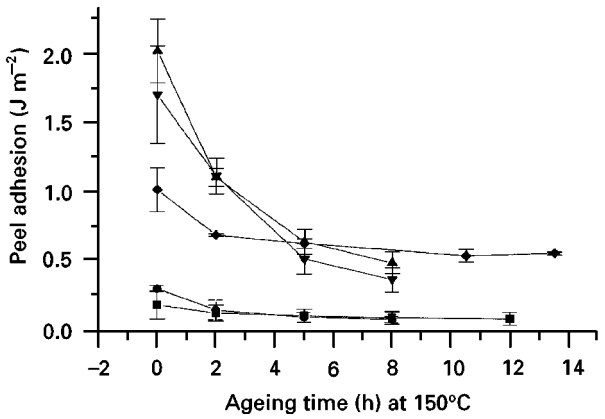

Figure 10 Peel strength results as a function of ageing time at 150 °C for the various copper interfaces evaluated. (■), specimen 1; (●), specimen 2; (▲), specimen 3; (▼), specimen 3A; (◆), specimen 3B.

shown by the dramatic drop-off in peel strength with time at elevated temperatures.

There was no clear difference in the fracture surfaces as a function of ageing time in the electron microscope. This would suggest that the failure mechanism is essentially the same irrespective of the period of elevated-temperature ageing. For the samples that were air oxidized, there is a clear transfer of oxidized metal to the polymer side, suggesting failure of the oxide to the base metal This would certainly explain the relatively poor strength values. The degradation in peel strength is most probably a function of how much oxide has fractured from the base metal during ageing relative to how much fractured during the peel test. If the base metal adhesion to the oxide is the limiting factor, it may also suggest why the ion-implanted and air-oxidized specimens had higher initial adhesion since some fraction of the weak link has been eliminated owing to the chromium sputtering when exposed to the ion implantation. There is some minimum level of resin still left on the aged metal surfaces, but there appears to be no large difference in peel strength as a function of ageing time.

Failure of the specimens made from the electroplated copper must be generally occurring beyond the base metal–oxide interface with generally higher overall adhesion. The rougher and more diffuse the interface, the more potential there is for a mechanical interlocking mechanism requiring polymer fracture where the resin enters the cavities of the metal surface or pull-out of those zones for interfacial debonding to occur. The use of benzotriazole as a surface coupling agent on the copper oxide did not significantly influence the amount of fracture to pull-out and no observable effect was observed.

Measurable differences are seen in the weaker response of the electroplated interfaces that were ion implanted. There are two explanations for the behaviour of these interfaces. One is that the ion implantation procedure is deleterious to the oxide formed during the plating operation which would enhance the ability of the resin to pull out of the mechanically interlocked surface. The other is that contamination would also serve to enhance pull-out. The influence of surface problems would be most easily manifested on the outer surfaces without the re-entrant cavities. The fact that the ion-implanted samples have collected a significant surface film of hydrocarbon prior to lamination may prevent epoxy resin interaction with the surface and lead to the formation of a more weakly bound resin. Adhesion may be still acceptable in regions where the re-entrant cavities have collected infiltrating resin because of the difficulty in pulling out resin from those zones. The formation of weakly bound zones that are mechanically interlocked may also explain why there is no apparent difference in the fracture morphology. Our results may have been different had we been able to laminate these specimens immediately following the ion implantation procedure. The lower initial peel strength for the electroplated and ion-implanted specimens could be attributed to some deleterious reaction between the other consitutents on the surface with the curing resin but that is not likely. Chromium at the surface could be an issue given other work on copper oxide surfaces formed by $NaOH–NaClO_2$ oxidation [23]. Of course, few have also looked at the issue of ion implanting into an oxide layer without performing a subsequent annealing step; so there may be a problem here also.

Ageing of these laminated interfaces at elevated temperatures reduced the peel strength. Given the level of roughness with the interfaces formed with these plated specimens, the residual stress state must be higher in these samples than in the other specimens that we have investigated. This suggests that a short-circuit pathway for failure exists around the tips of the nodules which leads to failure closer to the true interface. The results clearly show how problematic linking high adhesion to robust processing can be.

3.3. Kinetic analysis

Using the model approach, the peel strength data were analysed using a two-factor analysis including the long-term peel strength, $A(\infty)$, and the rate constant, Ω, in units of reciprocal hours. By maximizing the correlation coefficient using $A(\infty)$, the long-term adhesion, as a fit parameter, the degradation rate constant, θ, was determined from the analysis. From the analysis of each degradation curve, the results for the kinetics study could be compared and are shown in Table VI.

Two important points need to be made here. The first is that the different morphologies lead to different $A(\infty)$ values. The surface morphologies generated by processes 1 and 2 led to rather low $A(\infty)$ values while the electroplating treatment led to $A(\infty)$ values which were three to five times higher. This is understandable when one considers the mechanical interactions across the interface. The second point is that an inverse correlation was found between the oxide formation temperature and the initial peel strength. If there is a wide mismatch between thermal coefficients of expansion of the metal and the metal oxide, then residual stresses are likely to be high in the

TABLE VI Adhesion degradation kinetics modelling data

Process Type	Morphology	Oxidation	Surface modification	$A(\infty)$ ($N\,m^{-1}$)	Ω (h^{-1})	Correlation coefficient
1	Sanded	Air bake at 200 °C	None	0.079	0.43	0.99
2	Etched	Air bake at 200 °C	None	0.10	0.34	0.99
3	Egg shell	Plating	None	0.45	0.42	0.99
3A	Egg shell	Plating	Benzotriazole primed	0.29	0.37	0.99
3B	Egg shell	Plating	Ion implanted	0.51	0.15	0.90

oxide layer, and oxide fracture from the metal surface is likely.

If the adhesion of the base metal to the formed oxide is the weakest link in the interfacial construction, it makes little difference which surface enhancement is used. They will all lead to poor adhesion since failure occurs away from the location where ion implantation and primers were applied. This explains why, even though a different oxide is formed on the oxides formed by process 2, adhesion remains poor.

When considering the adhesion degradation of the electroplated copper interfaces, the large features in the morphology would only lead to decreased emphasis on the surface treatment. Failure of the epoxy–copper bond is occurring far from the true interface. The ion-implanted samples lead to failure to the true interface with substantially less degradation overall. It is suspected that the failure at long exposure times is due to the mechanical interlocking that remains. We also suspect that degradation is manifested as cracking in some of these mechanically locked regions, thus requiring failure of fewer regions during a peel test.

When the results of these experiments are compared with earlier reported results on copper surfaces treated with a hot alkaline oxidizing solution, $A(\infty)$ for these surfaces was consistently higher than even the initial laminated adhesion values for the air-oxidized specimens, regardless of the preparation method. This suggests that the presence of a weak boundary layer between the oxide and the base metal might preferentially fail and lead to evidence of low adhesion overall. When compared with the copper surfaces with the egg shell morphology, the $A(\infty)$ values are similar to although higher than those for plated surfaces. This suggests that there is some definitive reason to make a rougher topography, but the degradation rates are precipitously higher than for the samples made by the other treatment.

4. Conclusions

Different peel strengths were found between treatments that thermally oxidized copper on two different surfaces and a plating treatment designed to be significantly rougher than the other treatments. High peel strengths were observed between a high-temperature cross-linking epoxy resin and the plated surface while poor adhesion was observed on the thermally oxidized samples. It was found from this comparison that surface morphology plays a larger role in defining epoxy adhesion with copper than chemical bonding across the interface to a defined oxide. Different results may be obtained when all oxide forms have reasonable base metal adhesion.

We have reported similar degradation profiles in adhesion with elevated temperature ageing for other characteristic morphologies. Two completely different degradation mechanisms were found to be present; cohesive fracture at the base metal–oxide interface and fracturing through the high stress polymeric regions of the highly textured copper oxide morphology. Kinetic parameters associated with long-term adhesion and degradation rates were assigned.

Considering the adhesive strength of these oxidized copper interfaces with those of the previous work, there is an inverse correlation between the oxide formation temperature and the resulting adhesion. The internal stress in the formed oxide-base metal interface ultimately relates to adhesion when the interface fails preferentially.

References

1. D. J. ARROWSMITH, *Trans. Inst. Metal Finish.* **48** (1970) 88.
2. M. C. BURRELL and J. J. KEANE, *Surf. Interface Anal.*, **11** (1988) 487.
3. S. PIGNATARO, A. TORRISI and G. FERLA, *ibid.* **7** (1985) 129.
4. J. M. PARK and J. P. BELL, "Adhesion aspects of polymer coatings", edited by K. L. Mittal (Plenum, New York, 1983) pp. 205–224.
5. C. W. MILLER and P. C. LABERGE, *J. Vac. Sci. Technol. A.* **7** (1989) 1818
6. J. D. VENABLES, *J. Mater. Sci.* **19** (1984) 2431.
7. J. R. G. EVANS and D. E. PACKHAM, *J. Adhesion* **10** (1979) 177.
8. M. C. BURRELL, J. FONTANA and J. J. CHERA, *J. Vac. Sci. Technol A* **6** (1988) 2893.
9. A. J. KINLOCH, *J. Adhesion* **10** (1979) 193.
10. J. R. G. EVANS and D. E. PACKHAM, *ibid.* **9** (1978) 267.
11. L. J. SLOMINSKI and A. LANDAU, *Plat. Surf. Finish.* **69** (1982) 96.
12. H. K. YUN, K. CHO, A. H. AN and C. E. PARK, *J. Mater. Sci.* **27** (1992) 5811.
13. S. YOSHIDA and H. ISHIDA, *J. Adhesion* **16** (1984) 217.
14. H. ISHIDA and K. KELLEY, *ibid.* **36** (1991) 177.
15. N. INAGAKI, S. TASAKA and M. MASUMOTO, *J. Appl. Polym. Sci.* **56** (1995) 135.
16. J. DING, C. CHEN and G. XUE *ibid.* **42** (1991) 1459.
17. Q. DAI and Y. LU *Angew. Makromol. Chem.* **227** (1995) 121.
18. P. D. MUMBAUER, D. H. CAREY and G. S. FERGUSON, *Chem. Mater.* **7** (1995) 1303.

19. T. BRIDGE, R. P. M. PROCTOR, W. A. GRANT and V. ASHWORTH "Surface engineering". NATO Advanced study Institute Series, edited by R. Kossowsky and S. C. Singhal (Martinus Nijhoff, Dordrecht, 1984) pp. 209–227.
20. K. H. DIETZ, J. V. PALLADINO and A. C. VITALE, *Printed Circuit Fabrication* **13** (1990) 46.
21. T. A. TAM and R. D. ROBINSON, *Plat. Surf. Finish* **73** (1986) 74.
22. S. G. HONG and T. C. WANG, *J. Appl. Polym. Sci.* **52** (1994) 1339.
23. B. J. LOVE and P. F. PACKMAN, *J. Adhesion* **40** (1993) 139.

Received 25 April 1996
and accepted 7 July 1997